LUND UNIVERSITY

Experimental Investigation of the Directional Outdoor-to-In-Car Propagation Channel

Harrysson, Fredrik; Medbo, Jonas; Hult, Tommy; Tufvesson, Fredrik

LUND UNIVERSITY

PO Box 117
221 00 Lund
+46 46-222 00 00

Experimental Investigation of the Directional Outdoor-to-In-Car Propagation Channel

Fredrik Harrysson, *Senior Member, IEEE*, Jonas Medbo, Tommy Hult, *Member, IEEE*,
Fredrik Tufvesson, *Senior Member, IEEE*

Abstract—The demand for wireless channel models including realistic user environments is increasing. This motivates work on more detailed models that are reasonably simple and tractable but with adequate statistical performance. In this paper, we present an investigation of the spatial outdoor-to-in-car radio channel at 2.6 GHz. Specifically, we investigate the performance of a multiple antenna smartphone mock-up in the hand of a user. We evaluate and utilize a composite channel approach to combine measured antenna radiation patterns with an estimated spectral representation of the multipath channel outside and inside the car in two different scenarios. The performance of the method is investigated and comparisons with direct channel measurements are performed. Statistical and directional properties of the outdoor-to-in-car channel are presented and analyzed. It is found that the composite method, despite nearfield problems when estimating plane-wave channel parameters in a very narrow environment, constitutes a tool that provides reasonably viable statistical results. In addition, we have found that the introduction of the car in the propagation environment increases scattering and eigenvalue dispersion while it decreases pairwise antenna signal correlation. These statistical properties are found to slightly increase the possible diversity and the spatial multiplexing gains of multiple antenna terminals when located inside cars. This positive effect, however, is small compared to the negative effect of car penetration loss.

Index Terms—Mobile communication, channel models, propagation measurement, user phantom, multiple-input multiple-output (MIMO), vehicular channel, direction of arrival estimation.

I. INTRODUCTION

COMMUNICATION from vehicles have today become a prevalent scenario for handheld mobile terminals, such as smartphones, that may be in the hands of passengers using high data rate cellular services. This scenario will affect the tuning of the cellular networks and the quality-of-service of the cellular systems serving the users, and may also affect terminal technology. In addition, a car may also serve as a relevant example of an immediate confined scattering environment, representative also for other similar surroundings like indoor parts of buildings, other vehicles, trains, sub-ways, etc, that are common surroundings in the everyday life of mobile terminal users. Thus, in ubiquitous cellular systems, like LTE (long-term evolution) and future LTE-Advanced, it is of great interest to know in detail also the impact of such environments with respect to performance (power consumption, data rate, reliability etc.) of multiple antenna terminals such as MIMO (multiple-input multiple-output) smartphones. The car environment will have impact not only on the path loss which affects power consumption and coverage, but also on the fading statistics of the radio channel. Multiple antenna techniques such as diversity and spatial multiplexing, which are essential to combat fading and to boost channel capacity are also highly affected. However, channel models that, in a realistic way, incorporate these confined environments in the immediate neighborhood of the user are rare. Such channel models are of particular importance for the development of vehicular-to-infrastructure (V2I) solutions.

In the development of an empirical channel model that includes nearby scattering objects and surroundings it is possible to include the objects either in the representation of the antenna or in the propagation channel characterization. However, if these objects, e.g. a car, are included in the channel we need to perform new channel measurements for each configuration (terminal antenna, user orientation, car type, car orientation, location, etc.). Instead, by measuring the much more rigid outer channel once (at a representative location) we can produce a model that is represented by the *double-directional propagation channel* (DDPC), i.e., a sum of multi-path components (MPCs); each characterized by its direction-of-arrival (DoA), direction-of-departure (DoD), path delay, and complex amplitude [1]. The DDPC can be estimated from good quality MIMO channel measurements by methods like SAGE [2]. With the DDPC at hand, the outer channel can easily be combined with measured or simulated radiation patterns. This composite channel modeling (CCM) methodology is verified in [3–5] wherein it is also utilized to evaluate the influence of the body of the user. In the case of, e.g., an object large as a car, the method is still possible but perhaps not feasible or practical.

In this paper, we present an investigation of the influence of a standard family car on the spatial radio channel at 2.6 GHz, and specifically on the performance of a multiple antenna smartphone mock-up terminal in browse mode position in the hand of a user phantom. We utilize the composite channel approach where the user together with the antenna, is considered as one radiating unit or a *super-antenna* with the propagation channel represented both with the car absent and

inside the car. The environment inside a normal sized car does not, however, provide enough space to reach the far-field of a several wavelengths sized array antenna necessary for directional channel characterization, of a user phantom super-antenna, at relevant frequencies around 2.6 GHz. Thus, we have to violate the far-field requirement to use the in-car composite channel approach. Hence, the question is to what extent the composite method with the far-field assumption inherent both in the DDPC and in the super-antenna radiation pattern, is valid for MIMO performance prediction inside a car, and how much it suffers from the violation of the far-field assumption and (unavoidable) measurement inaccuracies.

Several published papers describe investigations of cars and other vehicles. Several papers also describe and evaluate the principle of combining a directional propagation characterization with antenna radiation patterns (here referred to as a composite channel modeling), e.g., [4, 6–8], but to our best knowledge no work exists that investigates and validates this composite channel modeling approach in a narrow confined scenario where, e.g. a mobile handset, in the presence of a user (phantom), is located inside a vehicle, e.g. a car.

The goal of the paper is to investigate to what extent the plane-wave spectrum composite channel method can appropriately account for a car environment with the mobile user inside.

In [9] we presented a measurement campaign and an initial investigation of the outdoor-to-in-car channel. Here we extend this analysis and present a new directional analysis of the channel that give us a tool to separate the specific effects of the user and the car. The novel contributions of the paper are the following:

1) We investigate the possibility of performing directional channel estimation from inside a car.
2) We compare the synthetic channel based on the estimated channel to direct measurements w.r.t. singular value distributions and antenna signal correlation in the presence of a user inside and outside the car.
3) We extend the analysis of the car environment (outdoor-to-in-car) with the directional analysis.
4) We analyze the specific influence of an upper body user phantom and the car environment, separately, on diversity and capacity performance of a four-antenna smartphone mock-up in browse mode.

The investigation is based on channel measurements in two different static scenarios with an upper body phantom and a four-antenna handset mock-up located outside and inside a common type family car (station wagon), in the LTE band 2.5–2.7 GHz for a synthetic 4×4 MIMO arrangement.

The paper is organized as follows: Section II outlines the basic principle of the composite method, Section III describes the details of the equipment, the test setup and the measurement scenarios, and Section IV elaborates on the measured channel properties and the directional characterization of the channel from inside the car. Next, the comparison procedure between direct measurements and composite results is described in Section V, with the comparison of eigenvalue distributions and antenna signal correlation as the key experimental results of the campaign. In Section VI we evaluate the impact of the car

on channel properties like correlation, diversity and capacity gain in different cases, and use the composite channel model to separate the user and the car influences. Finally, the paper is summed up and concluded in Section VII.

II. THE CHANNEL MATRIX

A. Channel Model

It is assumed that the radio channel can be modeled by a finite number L of multi-path components (plane waves), originating at the transmitter (Tx) antenna propagating towards the angle $\Omega_{t,l}$ (direction of departure), subject to reflection, scattering and diffraction, before terminating at the receiver (Rx) antenna impinging from angle $\Omega_{r,l}$ (direction-of-arrival). This means that the frequency domain MIMO channel transfer function (matrix) can be written as

$$\mathbf{H}(f) = \sum_{l=1}^{L} \alpha_l \mathbf{G}_r^T(\Omega_{r,l}, f) \mathbf{P}_l \mathbf{G}_t(\Omega_{t,l}, f) e^{-j2\pi f \tau_l}, \quad (1)$$

where α_l denotes the complex MPC amplitude, τ_l the path delay, and $\mathbf{P}_l$ the 2×2 normalized polarimetric transfer matrix. In (1) the assumptions is made that the antennas can be characterized by their far-field characteristics, i.e., that the closest MPC scatterer is outside the near-zone of the antenna. The antenna matrices $\mathbf{G}_t$ and $\mathbf{G}_r$ include also the complex array location vector phase term for each element in the columns, and for the polarization component (θ, ϕ) in the rows, i.e., $2 \times n_{r,t}$. Here we assume a static Rx unit which can be generalized to a dynamic case with the addition of the Doppler frequency by the substitution $f = (1 + \frac{v}{c_0})f_0$ in (1), where $v = \hat{k}_{r,l} \cdot \mathbf{v}$ is the Rx velocity relative the direction of each individual MPC $\hat{k}_{r,l}$ and c_0 is the speed of light.

The channel model in (1) can be modified for a case where the directional parameters are only important at the Rx side. In this case the channel model can be written as

$$\mathbf{H}(f) = \sum_{l=1}^{L} \mathbf{G}_r^T(\Omega_{r,l}, f) \mathbf{A}_l(f) e^{-j2\pi f \tau_l}, \quad (2)$$

where $\mathbf{A}_l(f) = \alpha_l \mathbf{P}_l \mathbf{G}_t(\Omega_{t,l}, f)$ is a $2 \times n_t$ matrix now containing polarimetric mutual complex amplitudes corresponding to the individual Tx antenna elements.

B. Channel Estimation and Calculation

With the channel model in (1) it is possible to calculate the channel matrix synthetically for any array antenna characterized by its farfield matrix $\mathbf{G}$ as long as the farfield assumption is not violated. When the channel model is used to represent an observation from a channel measurement, the channel parameters (DDPC parameters) $\boldsymbol{\theta} = \{\Omega_{t,l}, \Omega_{r,l}, \tau_l, \alpha_l, \mathbf{P}_l\}$ can be estimated by using a maximum-likelihood (ML) estimator that performs the operation

$$\hat{\boldsymbol{\theta}} \triangleq \arg\max_{\boldsymbol{\theta}} p(\mathbf{x}; \boldsymbol{\theta}), \quad (3)$$

where $p(\mathbf{x}, \boldsymbol{\theta})$ is the probability distribution function of the observed channel $\mathbf{x} = \text{vec}(\tilde{\mathbf{H}})$ and the parameter vector. It

can be shown that the log-likelihood function can be written as

$$-\log p(\mathbf{x};\boldsymbol{\theta}) = n_r n_t n_f \log(\pi\sigma^2) + \frac{1}{\sigma^2}\sum_{k=1}^{n_f} ||\tilde{\mathbf{H}}_k - \mathbf{H}_k||_F^2,$$
(4)

were k is the sample frequency index, σ^2 the noise variance, $\tilde{\mathbf{H}}$ is the channel model in (1), and $\mathbf{H}$ is a measurement realization.

The estimator used in this investigation is described in [10] (with reverse notation) and is here only described briefly. It starts by a search for the maximum in the power delay profile, followed by time-domain gating and dual-side beamforming to find initial parameter values ($\Omega_{t,l}$, $\Omega_{r,l}$ and τ_l) of the (multiple) MPC's within the selected delay slot. Next a binary search algorithm performs a binary tree search maximization to improve the parameter estimates one-by-one as in SAGE [2]. In a second step the estimation procedure performs an analytical gradient calculation, utilizing the multivariate quadratic Taylor expansion of the likelihood, to find the local maximum. In this step the Jacobian and the Hessian of the likelihood is calculated analytically. This step is very sensitive to model errors, e.g., due to non-planar wave fronts (while assuming planar wave fronts) when scatterers are to close to the sensor antenna array [11–13]. In Section IV-B this problem is further discussed.

These steps in the estimation procedure are iterated and combined with a linear estimation of $\alpha_l \mathbf{P}_l$, and with possible birth of new MPC's, until an accuracy threshold is reached and until the extraction of MPC's in the delay domain reaches the noise floor of the data. The estimation method is also mentioned in [14] and was used in [4, 15].

III. MEASUREMENT EQUIPMENT AND SETUP

A. Array antenna, Handset and User Phantom

In the experiments two different antenna configurations at the mobile side (MS) were used. One was a uniform cylindrical 64 element (4 rows, 16 columns) dual polarized square patch antenna array (receiving patch uniform cylindrical array, RxPUCA) to be used for directional estimation of the channel. The second was a handset mock-up with four (PIFA) antennas placed at the edges, connected by coaxial cables to a 1-to-4 switch. The handset is placed in the hand of a user phantom consisting of a liquid filled head-plus-torso and one solid (right) arm-plus-hand in *browse mode*. The user operation mode (browse mode) represents a smartphone mobile broadband scenario where the user watches the handset screen. Further details and pictures on handset and phantom can be found in [3, 4]. At the base station antenna side (BS), a uniform rectangular 4×8 dual polarized square patch antenna array (TxPURA) was used.

B. Car

The car is a 2005 model Volvo V70 station wagon with standard glazing and with the rear seats down-folded to make place for the antennas. The main investigation is made with the car empty from driver and passengers. Some additional
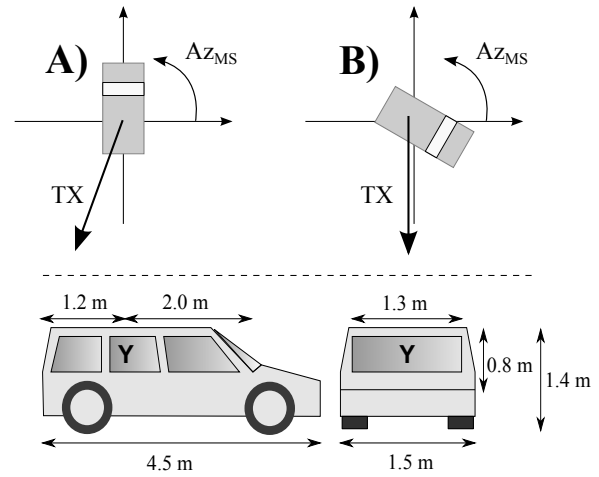

Fig. 1.   Orientation of the car in the two scenarios, and the car geometry with the location of the test antennas when inside the car.

TABLE I
CHANNEL SOUNDER PARAMETER CONFIGURATION DURING MEASUREMENTS.

Center frequency, f_c	2.6 GHz
Measurement bandwidth, B	60 MHz
Delay resolution, $\Delta\tau = 1/B$	16.7 ns
Transmit power, P_t	27 dBm
Test signal length, τ_{max}	1.6 μs
Number of TxPURA antenna ports, N_t	32
Number of RxPUCA antenna ports, N_r	128
Number of Rx handset antenna elements, $N_{r'}$	4
Snapshot time, $t_{snap} = 2 * N_t * N_r * \tau_{max}$	13.1 ms
Number of snapshots at each recording	100
Number of frequency samples	97
BS antenna height over ground, h_t	ca 9 m
MS antenna height over ground, h_r	1.1-1.3 m

measurements were done with a driver behind the wheel and with side windows open, but no significant effect due to the driver and the windows was found. The orientation of the car in the two scenarios is shown in Fig. 1 with the definition of the azimuth angle at the MS (Az_{MS}). The direction towards the BS is marked in both cases (about 250 degrees in Scenario A and 270 degrees in Scenario B). Also the geometry of the car and the placement of the channel sounder array antenna and the user phantom (inside the car) is shown.

C. Channel Sounder

The channel sounder used was the RUSK Lund channel sounder from Medav. The characteristics of the sounder setup are summarized in Table I.

D. Antenna Characterization

The radiation patterns and efficiencies of the handset, with and without the phantom present, have been measured previously [3, 4]. For the directional estimation we also needed a full characterization of the RxPUCA antenna. The calibration of the measurement array antenna is very important for

the accuracy of the directional estimation [16, 17]. This was measured in a high quality anechoic chamber with six meter separation between the transmitting dual polarized reference horn antenna, and the rotation center of the roll-over-azimuth positioning system.

In all channel measurements and syntheses described in this paper the same BS antenna (TxPURA) was used. Thus, since this antenna was unchanged in the channels that is being compared, directional estimations were only required at the MS side by using the modified channel model (2).

E. Channel Measurement Scenarios

Two measurement campaigns with two different MS location and orientation were performed at the Lund University Campus (E-building of LTH), Lund, Sweden:

- Scenario A: Parked car outdoor microcell scenario with line-of-sight (LOS) obstructed by a tree. The direction to the BS is towards the rear-left of the car with low elevation angle. Almost free sight through the rear window.
- Scenario B: Parked car outdoor microcell non line-of-sight (NLOS). The direction towards the BS is to the front-right of the car with buildings surrounding the car at three sides and obstructing the LOS.

In both scenarios the BS antenna was located at the same location (roof top of a two story building) with bore-sight towards the MS. In each scenario, two main configurations at the MS side were used. Firstly, the channel was recorded with the RxPUCA once for the purpose of directional channel characterization. Secondly, the channel was measured with the user phantom at the MS (user phantom plus handset) rotated in $90°$ steps to four orientations and translated to nine offset positions with $\lambda/2$ separation, i.e., 4×9 channel measurements in the latter case. These measurements were repeated twice in each scenario, once with the car absent but with the RxPUCA/phantom on a trolley at the MS location, and once with the RxPUCA/phantom placed inside the car at the nine MS locations. The measurements and scenarios are described with more details in [9].

The average receiver SNR (signal-to-noise ratio) for a single antenna to antenna (SISO) channel was between 0–17 dB in all measurements, which was improved almost 20 dB after coherent averaging over 100 channel snapshots recorded at each measurement. The measurements were taken during afternoons at a parking lot with almost no people and cars moving at the site. However, we cannot exclude that movements from a few passing pedestrians and cars in surrounding areas may have caused some interference.

IV. CHANNEL CHARACTERIZATION

A. Channel Characteristics and Estimated Parameters

With a bandwidth of 60 MHz corresponding to a standard resolution in delay of 5 meters we are not likely to resolve with good accuracy the possible impact on delay spread from the car presence by studying the power delay profile alone. However, by the high-resolution method described in Section II-B

TABLE II
CHANNEL PARAMETERS, DELAY SPREAD σ_τ, AZIMUTH SPREAD σ_ϕ AND ELEVATION SPREAD σ_θ, IN THE MEASUREMENT SCENARIOS, BASED ON THE ESTIMATED MPC PARAMETERS.

Scenario	σ_τ (ns)	σ_ϕ (deg.)	σ_θ (deg.)
A outside	54.9	24.6	7.1
A in car	63.3	39.1	13.6
B outside	45.1	33.4	29.2
B in car	51.2	45.4	27.4

we can improve the result. Having performed the channel parameter estimation we studied the results in the delay and directional domains, separately. Based on these estimates we calculated the corresponding channel properties, e.g., the rms delay spread σ_τ [18, Chapter 6] and the angular spread [19] in azimuth and elevation, S_ϕ and S_θ, respectively. These results are found in Table II and in Fig. 2 where the graphs show the directional distributions of estimated MPC parameters at the MS side for the different cases. From Table II we find that the delay spread increases slightly (about 6-8 ns) and that the azimuth spread increases significantly (about 12-15 degrees) when the antenna is located inside instead of outside the car in both scenarios. The vertical elevation spread, however, increases to some extent in Scenario A (the obstructed LOS case) while it is almost unchanged in Scenario B (the NLOS case). These observations of the angular spread are apparent by looking at the angular distributions in Fig. 2.

B. Channel Estimation Accuracy

An extensive number of uncertainties and possible error sources do inevitably affect the result of these evaluations. While some of these uncertainties are known and can be estimated, others are assumed to be negligible or small[1]. Below we discuss some of the most important error sources. Specifically, we illustrate with a few examples the consistency/inconsistency of doing plane-wave estimation in a propagation channel with near-field scattering sources, a topic that is central in this evaluation were we try to model a confined environment like the car.

1) Error sources and noise: The most important practical error sources in this investigation are most certainly the limited signal power strength (SNR) and limited antenna calibration (both arrays and phantom-plus-handset) measurement accuracy. During the channel measurements with the RxPUCA the internal LNA provides the SNR_{IR} of up to 50 dB after averaging over 100 coherent snapshots which is the peak-to-noise level of the input channel data to the channel estimation process in the outdoor cases, and about 42 dB inside the car in Scenario B.

The antenna measurement ranges used have a potential accuracy limit well below 25 dB, but due to practical compromises with switching, bending of cables, impedance mismatch, scattering in turntables, reconfigurability of phantom-plus-handset, etc., this error level is roughly about 20 dB

---

[1] A comprehensive investigation of experimental channel estimation limitations and various error sources can be found in [17]

(a) Scen. A outside

(b) Scen. A in car

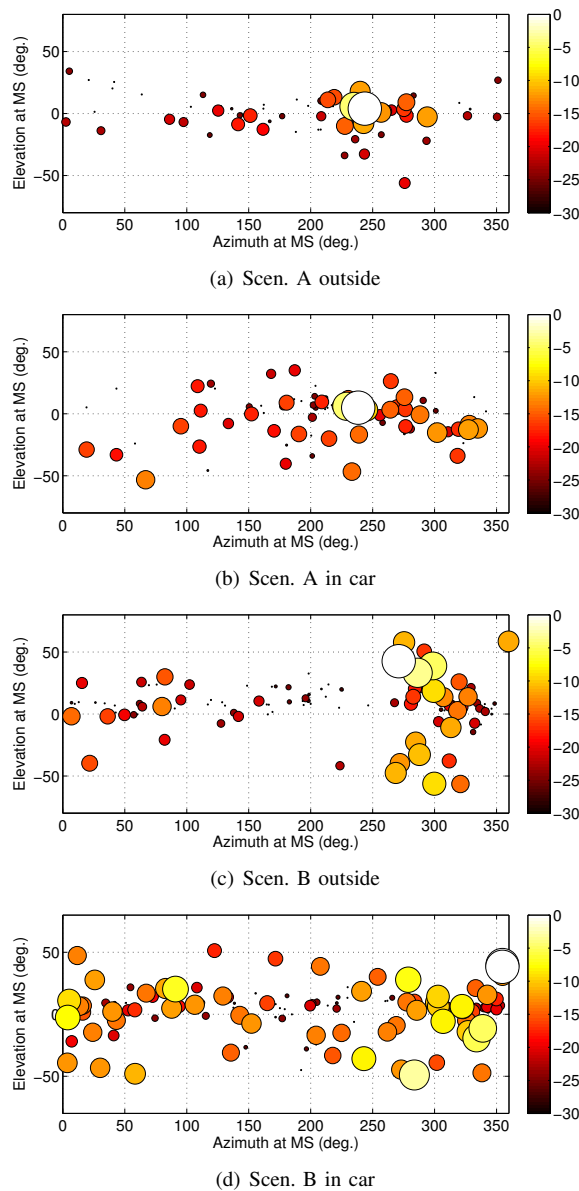(c) Scen. B outside

(d) Scen. B in car

Fig. 2.   Estimated MPC power vs. elevation and azimuth at the MS (DoA) in the different scenarios. The color of the circles represent the relative total power of the MPCs (dB).
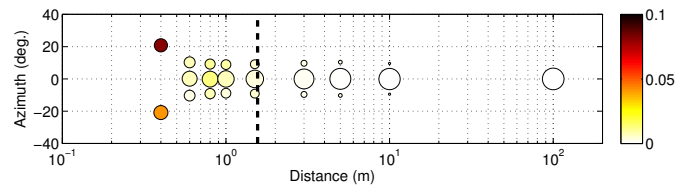

Fig. 3.   Estimated MPC azimuth angle to a single point source vs distance. The area of each circle is proportional to the MPC fractional power. The face colors of the circles show the estimated source distance minus the true test distance (m).

shown in Fig. 3. Here we used a theoretical model of the RxPUCA with Huygens sources and no mutual coupling. As seen from the graph the single source estimation degrade as the source distance decreases, with artificial sources appearing in directions corresponding to a spherical wave-front expansion on a plane-wave spectrum. We also observe an apparent source distance slightly larger than the actual one as the source approaches. The face colors of the MPC circles in the graph show the estimated (apparent) additional distance to the source.

However, by looking at Fig. 3 we also find that the ML estimation algorithm performs pretty good down to distances as low as 0.6 meters. This can be compared to the Rayleigh distance[2] ($2D^2/\lambda$ where D is the largest size of the antenna), which in our case is approximately 1.5 meters as marked in the graph. Thus, it does not seem impossible to estimate single sources with reasonable accuracy in our scenario, i.e., with a 0.3 m wide cylindrical array inside a common family car.

Now, what about angular resolution? To test this we add another source at the same distance as our first one but at a different angle. Since these two sources are at the same distance, the resolution in the far-field is simply the array beamwidth, i.e., roughly λ/D (rad.) or about 22 degrees. This effect is illustrated in Fig. 4. From the graphs it is apparent that when the angular difference gets close to the resolution limit, the estimation is valid only at source distances beyond the far-field distance, but at 45 degrees angular difference the estimation resolves the two sources even somewhat closer than the far-field distance but with an increased estimation error.

3) Estimation residual: The residual or remaining part of the channel after subtraction of the estimated MPCs, represents antenna calibration and channel model mismatch errors that are not possible to resolve[3]. This level relative to the peak level of the impulse response is referred to as the estimation *accuracy*. With the MS array outdoors this level was about 20 dB after channel parameter estimation in both scenarios, but with the MS inside the car it was less than 10 dB. The latter depends (most certainly) on the channel model mismatch, and the question is whether these results are useful nevertheless. This is discussed below.

[2]far-field or Fraunhofer region [20]
[3]Non-resolvable MPC's are sometimes referred to as non-specular or diffuse multipath components (DMC)[16,17]. In this work we make no distinction between specular and non-specular MPCs.

below the peak for the RxPUCA used for directional channel estimation, and minimum about 10 dB for the phantom-plus-handset antennas. The expected minimum accuracy level of the estimated MPCs is somewhere between 20-30 dB.

2) Nearfield estimation effects: Inside the car the closest obstacles or sources of scattering are within about 40 cm distance from the sounder array antenna center, see the car geometry in Fig. 1. However, if we neglect the car ceiling in the direction of elevation angles above 60 deg, where this antenna is unlikely to detect MPCs, the closest obstacles are at distances beyond 60 cm. Thus, we would like to be able to estimate MPCs at least at this distance, $d_l = c_0 \cdot \tau_l$, with reasonable angular and distance accuracy. To test this, we performed channel parameter estimation on a synthetic test channel with a single vertically polarized point-source at zero elevation and distances between 0.3–10 meters. The result is
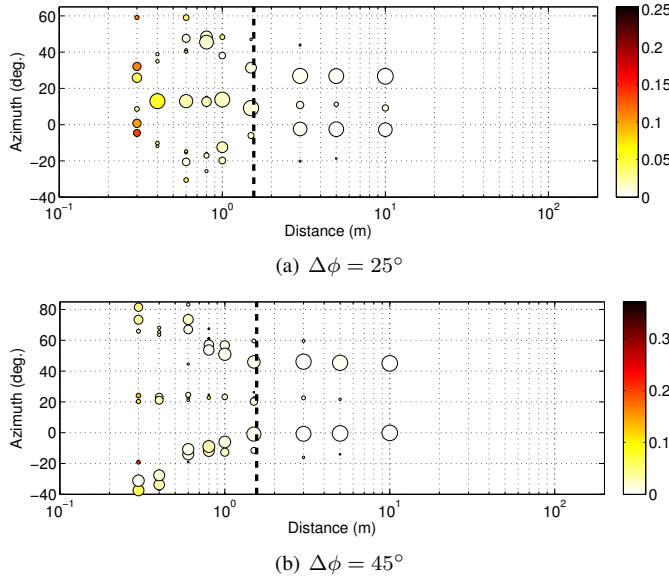
(a) $\Delta\phi = 25°$

(b) $\Delta\phi = 45°$

Fig. 4. Two estimated MPCs with different azimuthal separation $\Delta\phi$ vs true test source distance. The area of the circles is proportional to the fractional power. The face colors of the circles show the estimated source distance minus the true test distance (m).

TABLE III
COMPARISON OF AVERAGE RECEIVED SIGNAL POWER BETWEEN MEASUREMENTS AND MODEL FOR TWO ARRAY COLUMNS (WEAKEST AND STRONGEST SIGNAL) OF THE TEST ARRAY (RxPUCA) IN THE FOUR CHANNELS WITH SEPARATION W.R.T. CO- AND CROSS POLARIZATION OF BS AND MS ANTENNAS.

Scenario	ϕ_{col}	Pol.	P_{col}^m (dB)	P_{col}^c (dB)	Diff. (dB)
A outside	max	co	-74.3	-74.5	0.2
		cx	-91.2	-93.4	2.2
	min	co	-80.7	-81.2	0.5
		cx	-93.2	-96.3	3.1
A in car	max	co	-79.1	-79.3	0.2
		cx	-88.4	-91.7	3.3
	min	co	-83.2	-83.9	0.7
		cx	-89.3	-93.1	3.8
B outside	max	co	-76.6	-76.8	0.2
		cx	-87.1	-88.8	1.7
	min	co	-80.2	-81.0	0.8
		cx	-89.8	-92.2	2.4
B in car	max	co	-83.4	-84.6	1.2
		cx	-86.6	-90.0	3.3
	min	co	-84.3	-86.2	1.8
		cx	-88.3	-91.5	3.3

V. COMPARISON BETWEEN MODEL AND MEASUREMENTS

Based on the measured channels and the estimated directional channel parameters, the specific impact of the car presence in the outdoor-to-in-car channel can now be evaluated. But first we need to validate the method to be used.

A. Channel Matrix Element Magnitudes

A first step in the validation of both the direct measurements themselves, and the performance of (1), using the channel parameter estimations outside and inside the car, is to look at and compare the average received powers of individual antenna elements at the mobile (Rx) side. Here we let the average received power level for individual elements P_i at the receiver side be represented by the squared magnitude of the elements of the channel matrix $\mathbf{H}$ averaged over the TX antennas and the frequency as

$$P_i = \frac{1}{n_t, n_f} \sum_{j=1}^{n_t} \sum_{k=1}^{n_f} |H_{i,j,k}|^2 \qquad (5)$$

In Table III the average power P_{col} at two selected columns of the RxPUCA is compared for the direct channel measurements P_{col}^m and the channel synthesis calculation by (1) P_{col}^c. In general the differences between the channel synthesis and the direct measured results are due to the truncation by the ray estimation process not catching all the measured channel energy, the limited estimation accuracy due to model errors (especially inside the car where a higher degree of cylindrical and/or spherical wave propagation are likely), and the limited antenna calibration accuracy. The preserved energies by the model were here found to be 92, 74, 83, and 59 percent in the four cases, respectively, i.e., in Scenario A outside and

inside the car, and in Scenario B outside and inside the car[4]. This was found as the fraction between the synthetic and the measured overall average channel gains $\overline{P}_c/\overline{P}_m$ where

$$\overline{P}_{(m,c)} = \frac{1}{n_r, n_t, n_f} \sum_{i=1}^{n_r} \sum_{j=1}^{n_t} \sum_{k=1}^{n_f} |H_{i,j,k}^{(m,c)}|^2$$
$$= \frac{1}{n_r n_t n_f} \sum_{k=1}^{n_f} ||\mathbf{H}_k^{(m,c)}||_F^2 \qquad (6)$$

where $\mathbf{H}_k = \mathbf{H}(f_k)$. Since we test the channel model with the same array antenna model (measurement data) that was used in the channel estimation process, the lost energy must be due to the estimation loss or residual if the antenna characterization is at least approximately correct and span the same dimensions (polarizations, number of elements and position). From Table III we find that the difference in average power level between the model and the measurements differs quite a bit for different test antenna columns in different channels. Clearly the error gets larger as the signal gets weaker. In the highly directive channels, i.e., A outside, A in car, and B outside, the difference is as low as 0.2 dB for co-polarized antennas when the antenna column are directed towards the main DoA (strongest signal), and as high as 3.8 dB in the worst case (cross polarization in A in car) when the column is turned away from the main DoA. In the NLOS case (B) inside the car, the difference is somewhat higher (and the signal weaker).

From these data we also observe that the cross polarization seems to increase significantly from outside to inside the car. This effect is underestimated by the model due to the inability (truncation) to estimate the weak cross polarized signals from opposite the main DoA.

[4]These figures depend to some extent on the parameter setting in the estimation process
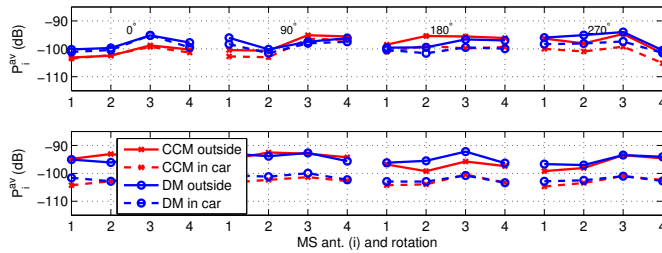
Fig. 5. Average received signal powers of individual antenna elements of the phantom user with the smartphone mock-up for vertical polarization at the BS. The upper graph show the result in Scenario A and the lower in Scenario B.

TABLE IV
AVERAGE RECEIVED POWER FOR THE MEASUREMENTS AND THE MODEL, DIFFERENCES, AND THE RMS ERRORS FOR THE PHANTOM-PLUS-HANDSET CASE IN THE FOUR SCENARIOS.

Scen.	$\overline{|H_{i,j}^m|^2}$ (dB)	$\overline{|H_{i,j}^c|^2}$ (dB)	Δ_{dB}	σ_{dB}^2
A outside	-97.5	-101.8	4.3	0.15
A in car	-99.1	-104.5	5.4	0.06
B outside	-93.1	-98.9	5.8	0.04
B in car	-101.0	-107.1	6.1	0.01

In the next step this validation of channel synthesis is done also for the case with the phantom user and the four-antenna handset. In this case we also utilize the nine offset positions and the four horizontal rotations of the phantom outside and inside the car to improve statistics. The result is shown graphically in Fig. 5 with the average power levels compared between the measured and the synthetic data on the ordinate for vertical polarization at the MS side, and with the four handset antennas and the four phantom rotations on the abscissa. Here the average power of the synthetic channels was set equal to the average power of the directly measured channels outside the car. Thus, no power loss due to truncation of estimated MPC's are present. Also here we find a good match between the synthesis and the direct measured data. The differences are, again, due to limited estimation accuracy, and here also the limited accuracy of the phantom-plus-handset antenna patterns due to reassembly of the user phantom and handset setup with non-identical bending of cables and positioning of the handset in the phantom hand. The mean received power, the difference Δ_{dB}, and the root-mean-square (rms) σ_{dB}^2 of the relative error are summarized in Table IV. Here no equalization of the average powers is done, and, hence, a notable bias error Δ_{dB} is revealed. This difference in mean is partly due to the truncation loss of estimated weak specular rays and possibly also irresolvable or non-specular (diffuse) channel components, and partly due to an additional cable loss of approximately 2 dB due to cables used in the channel measurements but not in the antenna calibration. The relative error is here taken as

$$\epsilon_i = \frac{P_i^c - P_i^m}{P_i^m}, \tag{7}$$

where i represents a compound antenna element and phantom rotation index. The mean and the rms are calculated as

$$\overline{\epsilon} = \frac{1}{n_r n_{rot}} \sum_{i=1}^{n_r n_{rot}} \epsilon_i \tag{8}$$

$$\sigma_\epsilon = \sqrt{\frac{1}{n_r n_{rot}} \sum_{i=1}^{n_r n_{rot}} (\epsilon_i - \overline{\epsilon})^2}, \tag{9}$$

and the transform to decibel is done as $\sigma_{dB}^2 = 10 \log_{10} |1 + \sigma_\epsilon^2|$. The very small rms error in Table IV indicates a good match or similarity between the synthetic channel

and the direct measurements, even though this apparent accuracy is partly an effect of the average power being not so sensitive to the antenna pattern and the phantom rotation. To a large extent it is still the efficiency of the individual antennas at the handset in the proximity of the user that sets the received power levels.

B. MIMO Eigenvalue Distribution

The most important statistical properties of a MIMO channel matrix regarding capacity performance are given by the singular values of the corresponding channel matrix. The squared singular values are equal to the eigenvalues of the channel covariance matrix

$$\boldsymbol{\lambda} = \text{eig}\{\mathbf{H}\mathbf{H}^H\} \tag{10}$$

and represent signal gains of the spatial sub-channels. Again, to validate the directional channel parameter estimations and the composite channel approach, outside as well as inside the car, the sorted singular value distributions for 32×32 test channels in the four scenarios are plotted in Fig. 6. With these test matrices each array ring, 32 antenna ports of the 128 elements RxPUCA, is treated separately as four samples of the same channel. The singular value distributions are shown for both directly measured channels, and composite channel models with and without the presence of the car, in both cases with normalization to unit channel gain (squared Frobenius norm). Naturally the composite channel data based on the estimated channel parameters are somewhat more "synthetic" with larger eigenvalue dispersion or, equivalently, less channel richness. Apparently, there is a pretty good statistical match between the model and the measurements also inside the car for the stronger eigenvalues. The weaker eigenvalues are very unreliable and reflect measurement noise as well as measurement and model (estimation) errors. The number of estimated MPCs was here maximum $L = 100$.

In the next step this validation of the channel synthesis is done also for the case with the phantom user holding a smartphone mock-up handset. In this case we utilize the nine offset positions and the four horizontal rotations of the phantom outside and inside the car to improve statistics. Here we allow ourselves to add an i.i.d. noise matrix $\mathbf{H}_w \sim \mathcal{CN}(\mathbf{0}, \sigma_w^2 \mathbf{I})$ to the synthetic channel matrix as

$$\mathbf{H}_c' = \mathbf{H}_c + \mathbf{H}_w. \tag{11}$$

By this procedure we compensate for inevitable receiver noise in the measurement system inherit in the direct measured data
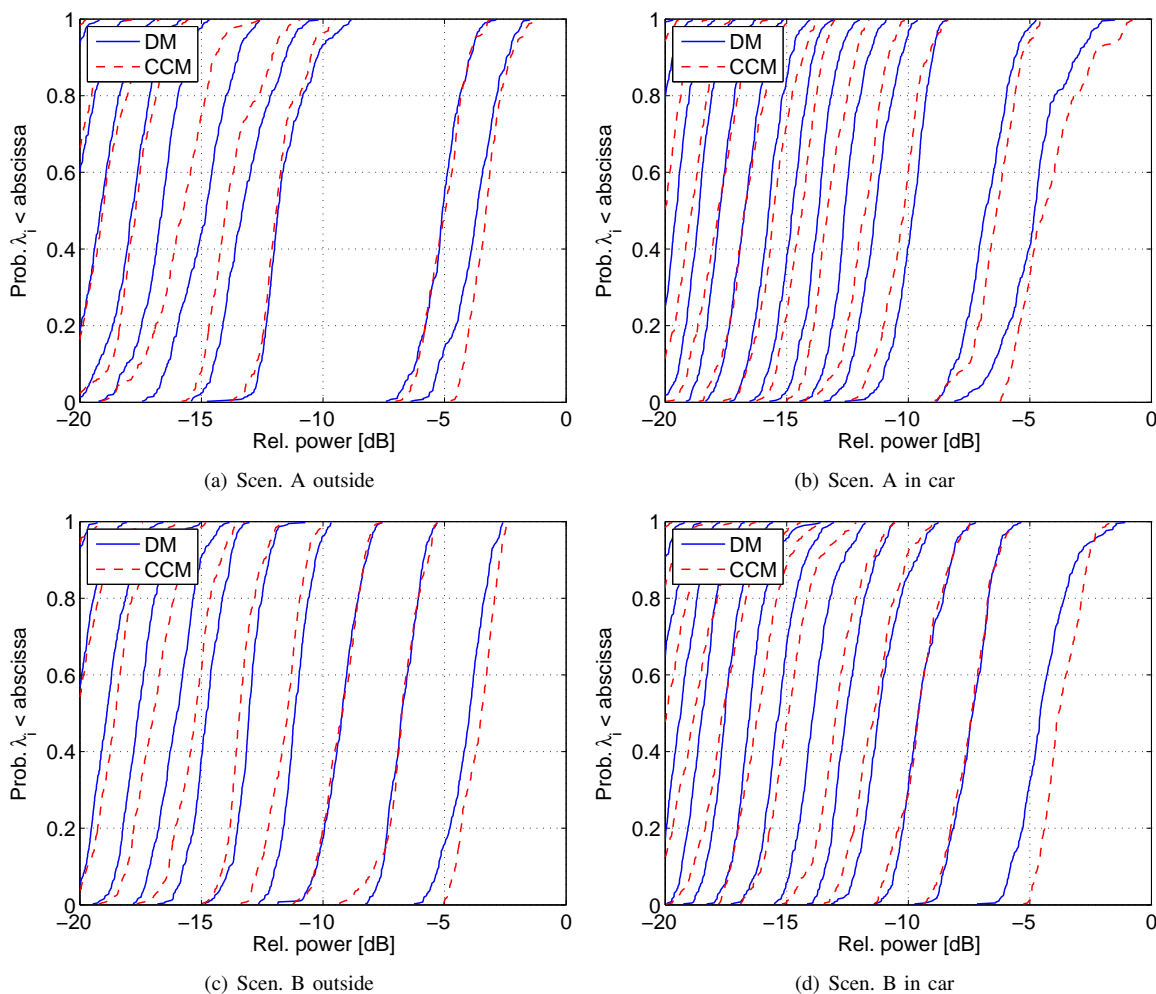
Fig. 6. Ordered squared singular value distributions of 32×32 channels for direct measured (solid), and CCM (dashed) with the RxPUCA in the four scenarios. Note that only the strongest singular values are visible.

and indirect present in the synthetic channel by setting the lower limit of MPCs to be estimated. The noise power σ_w^2 used in (11) was estimated from the channel measurements by comparing successive snapshots, resulting in an estimated noise power $\hat{\sigma}_w^2$ so that the average SISO channel SNR of the direct measurements become $\overline{||\mathbf{H}_m||^2}_F/(n_r n_t \hat{\sigma}_w^2) = [18.5\ 16.9\ 26.9\ 19.0]$ dB in the four channels "A outdoor", "A in car", "B outdoor", and "B in car", respectively. In the delay domain this corresponds to a peak-to-noise floor level of the impulse response $\text{SNR}_{IR} \approx 40$ dB. The estimated channel sounder measurement noise power $\hat{\sigma}_w^2$ can also be removed from the total signal powers evaluated in the previous section (Section V-A), as is described in [17, Eq. (10)], to reduce the noise contamination. However, here this effect was found to be insignificant.

The result is shown in Fig. 7. At the BS side a selection of four vertically polarized antenna elements with $\lambda/2$ spacing was chosen from one row of the TxPURA. The match between the synthetic channel and the measured is close for all four singular values in all four scenarios. Especially inside the car the match is almost perfect in the NLOS case (Scenario B). This may partially be a consequence of that estimation errors

provide an apparent realistic spatially rich channel in this specific case, the one with most rich scattering, see Fig. 2. Otherwise, the additive noise has a minor effect on the result so the main difference between the synthetic and the measured channels is the lack of richness in the synthetic channel that stems from the inability to estimate enough MPCs due to limited SNR and error level. To improve these results we need higher SNR in the measurements and perhaps also higher accuracy in the antenna characterization and system calibration including cables etc. The addition of the noise matrix $\mathbf{H}_w$ in this context shall *not* be mistaken as an additive part of the channel model. The improved match with the direct measured channel is merely a consequence of the imperfect measurement system (receiver noise), but may also compensate for error sources like antenna array characterization and cable calibration errors, as well as for non-resolvable *spatially white* channel components. In [16, 17] the channel model itself is divided into a specular and a non-specular part, where the latter part (dense multipath) encounters possibly correlated non-specular channel components that are estimated separately. Here we persist in using the spectral channel model in (1) built up by classical independent specular components that may be
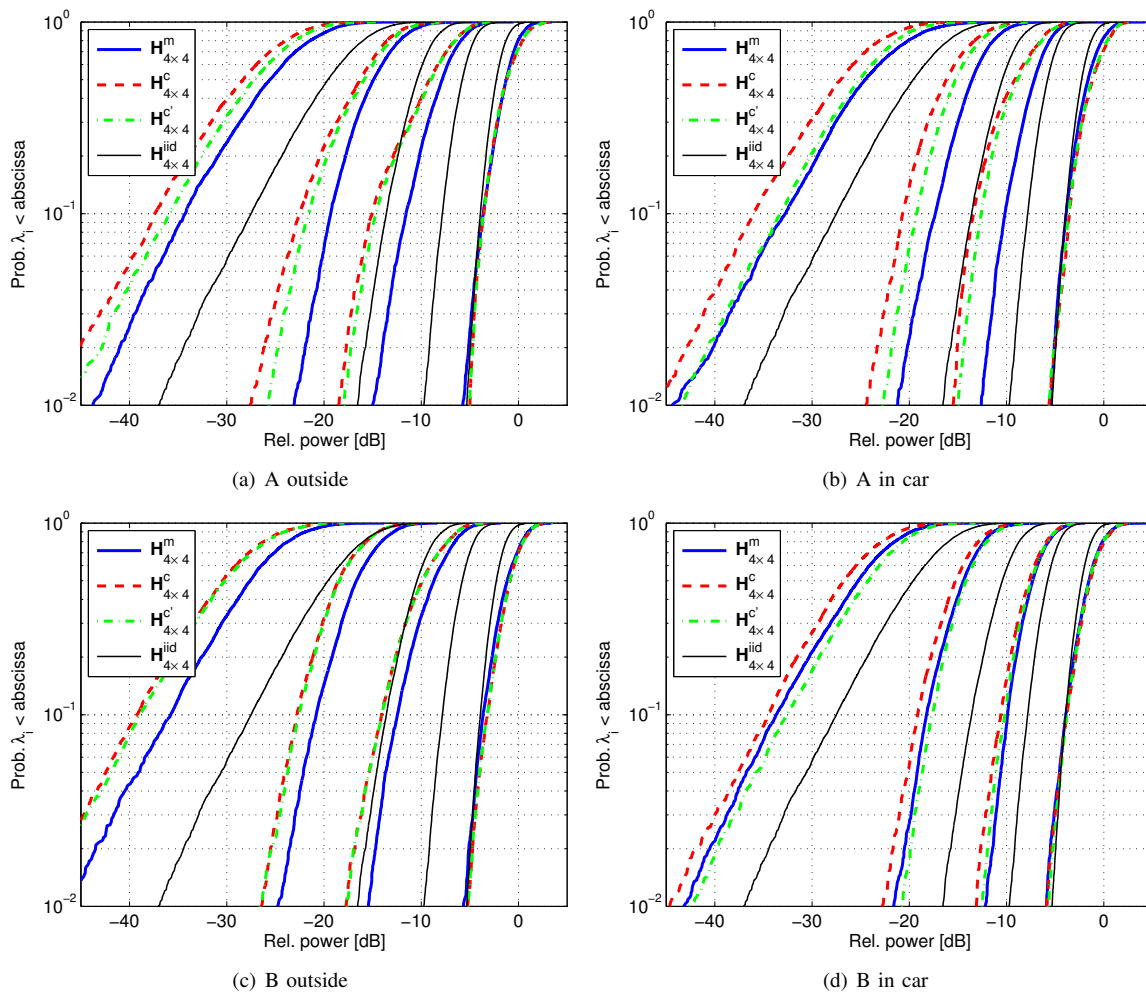
Fig. 7. Ordered squared singular value distributions of 4×4 channels for direct measured (m), and synthetic with the phantom-plus-handset (c and c'), in both scenarios outside and inside the car. For comparison the distribution of an i.i.d. complex Gaussian channel is shown (iid).

resolvable or not depending on the quality of the measurement setup and the estimator algorithm. In [4] higher precision in similar measurements provided the possibility to extract a higher amount of specular channel components which showed an increased match between the synthetic and the direct measured channels as the number of specular components increased. This effect was not reached by adding spatially white noise.

VI. How the User and the Car Affect System Performance

Since the composite channel model based on the MPC estimations work well in predicting the statistical properties of the MIMO channel, the tool can be used to extract and evaluate specifically how the user and the car affect system performance without further measurements. Some of these results were presented in [9], but now by utilizing the channel modeling tool it is also possible to separate the user and the car effects by comparing the synthetic channels for the handset plus user phantom with new channel calculations with previously measured handset only antenna patterns (as was done in [4] in an office environment). The handset patterns are

first translated and rotated to the same position as if they were in the hand of the user phantom. In a previous investigation of user effects it was found that one of the main characteristics of the user body was an increase in correlation between received signals from the handset antennas [4], in turn affecting system properties such as diversity and channel capacity.

A. Antenna Correlation in Channel

The antenna (signal) correlation can be found directly from the direct measurements and was presented in [9], but here we also want to compare with the results found by synthesis. The correlation matrix with entries $R_{i,j}$ denotes the correlation between signals at receive antenna ports i and j and can be estimated as the mean over frequency samples[5] of the sample covariance matrix

$$\mathbf{R} = \frac{1}{n_f n_t} \sum_{k=1}^{n_f} \mathbf{H}(f_k)\mathbf{H}^H(f_k) \tag{12}$$

[5] assuming ergodicity in frequency and time, i.e., averaging over the ensemble is equivalent to averaging over time- and frequency-samples [21]
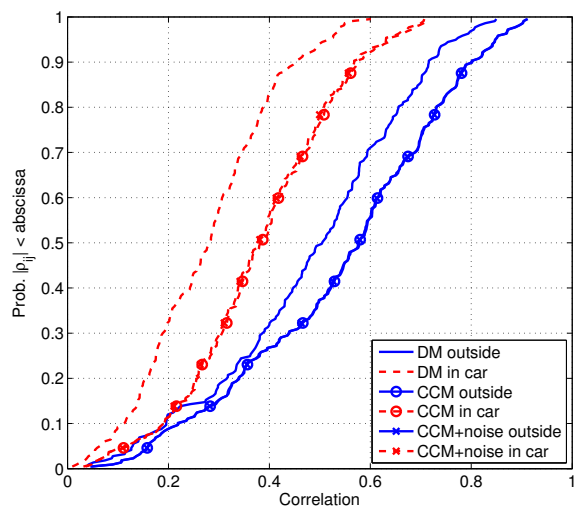
Fig. 8. Cumulative distribution of the estimated MS antenna correlation coefficient for the phantom-plus-handset outside and inside the car in Scenario B (NLOS) for direct measurements (DM) and synthetic (CCM) results.

giving the estimated complex correlation coefficient with the proper normalization as

$$\rho_{i,j} = \frac{R_{i,j}}{\sqrt{R_{ii}R_{j,j}}} \qquad (13)$$

Fig. 8 shows the cumulative distribution of the magnitude of the complex correlation coefficients computed according to (13), where the ensemble is the slow (shadow) fading distribution, i.e., the four phantom rotations, and the nine offset locations. In the figure the correlation coefficients from the synthetic channel model ("CCM"), with and without the noise compensations from (11), and from the direct measurements for the ensemble of $\rho_{i,j}$ are compared for all $i \neq j$. The presence of the car decreases the antenna correlation in the test channels, most likely due to increased scattering "richness" inside the car [9]. This effect is also reflected by the synthetic data even though these data show higher correlation in general. Nevertheless, we may conclude that the effect of the car is well caught by the model. The maximum difference in average received power between antenna elements was here about 2.5 dB, a figure sometimes referred to as antenna mismatch (not to be confused with impedance mismatch).

B. Diversity and Capacity Gain

A summary of the maximum-ratio combining (MRC) diversity gains and the capacity (or spatial multiplexing) gains are presented in Table V. Here the diversity gain (DG) is taken as the ratio of the combined signal power of the two strongest (DG2) and all four (DG4) antennas, to the strongest branch single antenna signal power at the 1% outage level. This diversity gain is also referred to as the apparent diversity gain [22] and seem to slightly overestimate the actual diversity gain [23, Fig. 11], where the latter definition refers the gain to a reference case with a truly isolated single antenna and, thus, omits the influence of mutual coupling by the surrounding terminated elements in our case. This effect is here neglected.

TABLE V
SUMMARY OF DIVERSITY GAIN (dB) AND CAPACITY GAIN (BITS/S/HZ) FOR THE DIFFERENT SCENARIOS AND CONFIGURATIONS.

Scen. A/B	Outside no user	Outside with user	In car no user	In car with user
DG2 (1%)	10.1/10.7	9.2/9.7	9.9/10.3	9.6/10.2
DG4 (1%)	16.0/17.3	14.4/15.2	16.5/17.2	14.8/16.8
ECG 4×2	2.0/2.4	1.7/2.4	2.4/2.7	2.1/2.6
OCG 4×2	2.3/2.1	1.8/1.6	2.5/2.1	1.8/2.1
ECG 4×4	4.1/4.7	3.5/4.6	4.7/5.5	4.4/5.2
OCG 4×4	3.6/4.3	3.3/4.0	4.4/4.9	4.2/4.7

The channel capacity is calculated from the eigenvalues of the normalized channel matrix as

$$C = \sum_{i=1}^{r} \log_2(1 + \gamma_i \lambda_i), \qquad (14)$$

where r is the rank of $\mathbf{H}$, and γ_i is the SNR after power allocation (by waterfilling assuming channel knowledge at the transmitter) to the sub-channel corresponding to λ_i and with SNR= $\sum_{i=1}^{r} \gamma_i$. The channel matrix is normalized with the square-root of the SISO channel power averaged over the sample space (here the frequency samples, rotations and small-scale translations) in each scenario and handset/user/car configuration. Thus, the average user efficiency and car penetration loss is omitted and only statistical and individual antenna properties of the channel are considered.

From the distribution of C over the sample space, the ergodic capacity gain (ECG) is taken as the difference between the mean MIMO capacity and the mean of the best SIMO capacity, while the outage capacity gain (OCG) is taken at 10% outage level. The 4×4 channel matrix is formed by selecting four vertically polarized antenna elements in the bottom row with one wavelength spacing at the BS, and in the 4×2 case the two single MS antennas that provide the highest overall capacity is selected. The SNR was set to 10 dB.

The diversity and capacity results in Table V show only minor effects of the user and the car environments when the impact of body loss and car penetration loss are absent. Both the diversity gain and the capacity gain are somewhat higher in Scenario (B) compared to the Scenario (A). The user presence seems to have a negative impact on both these measures which were also found in [4], while the car environment increases the performance of spatial multiplexing up to 0.9 bits/s/Hz for the 4×4 system.

VII. CONCLUSIONS

The purpose of this investigation of an outdoor-to-in-car radio channel at 2.6 GHz has mainly been two-fold: i) to investigate the validity MIMO composite channel model (CCM) formed by a combination of a the directional propagation channel and the far-field radiation patterns of array antennas, with respect to MIMO performance, and ii) to evaluate the possibility to (accurately enough) perform directional channel estimation in the close confined car environment.

Two outdoor measurement campaigns have been performed where, specifically, the influence of a car is considered at

the mobile side. From the measurements with a cylindrical array antenna, directional channel parameter estimation was performed to form the propagation channel model as a part of the composite channel model. Combined with measured antenna patterns of the handset-plus-user it is found that this channel model produces channel properties such as path loss and channel statistics very similar to what are found by the direct measurements with the handset-plus-user in the channel. The composite channel model shows lower eigenvalue dispersion and higher antenna branch correlation as compared to the direct measurements. This is assumed to be an effect of the limited channel parameter resolution due to measurement noise and calibration errors.

The main challenge with the investigation was the directional estimation inside the car where parts of the car and, thus, possible sources of interaction (scattering) are within the far-field or Rayleigh distance of the antenna. Tests of the estimation algorithm on a single point source and two separated (in angle) point sources at a certain distance with a representative theoretic array antenna (to avoid antenna array calibration errors) show potential problems as the sources get within distances from the antenna about the size of the car. Despite this violation we find that the directional estimation inside the car produces reliable results, both regarding the angular distribution of the MPCs, as well as the singular value distributions of the composite channel. Thus, we conclude that the main specular components of the channel seem to account also for the most important statistical properties, and that the CCM *can* be used to model the outdoor-to-in-car channel.

Finally, with the CCM at hand, the specific influence of the car and the user was evaluated both separately and in combination. Apart from the penetration loss of the car (in average between 2-8 dB) or in an interference-limited scenario, our results show little influence of the user and the car on the channel. Both diversity gain and capacity gain are found to be slightly higher in Scenario B compared to Scenario A, the user seems to decrease these measures, while the car environment increases the capacity (at fixed SNR) by up to 0.9 bits/s/Hz for the 4×4 system.

References

[1] M. Steinbauer, A. F. Molisch, and E. Bonek, "The double-directional radio channel," *IEEE Antennas Propagat. Mag.*, vol. 43, no. 4, pp. 51–63, Aug. 2001.

[2] J. A. Fessler and A. O. Hero, "Space-alternating generalized expectation-maximization algorithm," *IEEE Trans. Signal Processing*, vol. 42, no. 10, pp. 2664–2677, Oct. 1994.

[3] F. Harrysson, J. Medbo, A. F. Molisch, A. J. Johansson, and F. Tufvesson, "The composite channel method: Efficient experimental evaluation of a realistic MIMO terminal in the presence of a human body," in *IEEE Veh. Technol. Conf. VTC 2008-Spring*, Singapore, May 2008, pp. 473–477.

[4] ——, "Efficient experimental evaluation of a MIMO handset with user influence," *IEEE Trans. Wireless Commun.*, vol. 9, no. 2, pp. 853–863, Feb. 2010.

[5] M. Käske, C. Schneider, W. Kotterman, and R. Thomä, "Solving the problem of choosing the right MIMO measurement antenna: Embedding/de-embedding," in *Proceedings of the 5th European Conference on Antennas and Propagation (EUCAP)*, Apr. 2011, pp. 2551 –2555.

[6] A. F. Molisch, M. Steinbauer, M. Toeltsch, E. Bonek, and R. S. Thomä, "Capacity of MIMO systems based on measured wireless channels," *IEEE J. Select. Areas Commun.*, vol. 20, no. 3, pp. 561–569, Apr. 2002.

[7] P. S. Suvikunnas, J. Villanen, K. Sulonen, C. Icheln, J. Ollikainen, and P. S. Vainikainen, "Evaluation of the performance of multi-antenna terminals using a new approach," *IEEE Trans. Instrum. Meas.*, vol. 55, no. 5, pp. 1804–1813, Oct. 2006.

[8] M. Käske, C. Schneider, R. Thomä, and J. Pamp, "Application of the channel synthesis approach to evaluate the performance of an experimental 4-port application antenna," in *Proceedings of the 6th European Conference on Antennas and Propagation (EUCAP)*, Mar. 2012, pp. 11 –15.

[9] F. Harrysson, T. Hult, and F. Tufvesson, "Evaluation of an outdoor-to-in-car radio channel with a four-antenna handset and a user phantom," in *IEEE Veh. Technol. Conf. VTC 2011-Fall*, San Francisco, CA, Sep. 2011.

[10] J. Medbo and F. Harrysson, "Efficiency and accuracy enhanced super resolved channel estimation," in *Antennas and Propagation (EuCAP), Proceedings of the 6th European Conference on*, Prague, Czech Republic, Mar. 2012.

[11] K. Haneda, J.-I. Takada, and T. Kobayashi, "Experimental evaluation of a SAGE algorithm for ultra wideband channel sounding in an anechoic chamber," in *International Workshop on Ultra Wideband Systems, Joint UWBST IWUWBS*, Kyoto, Japan, May 2004, pp. 66–70.

[12] M. Landmann and J.-I. Takada, "On the plane wave assumption in indoor channel modelling," in *IEICE Society Conference*, Sapporo, Japan, Sep. 2005, pp. B–1–207.

[13] K. Haneda, J.-I. Takada, and T. Kobayashi, "A parametric UWB propagation channel estimation and its performance validation in an anechoic chamber," *IEEE Trans. Microwave Theory Tech.*, vol. 54, no. 4, pp. 1802 – 1811, Jun. 2006.

[14] J. Medbo, M. Riback, H. Asplund, and J.-E. Berg, "MIMO channel characteristics in a small macrocell measured at 5.25 GHz and 200 MHz bandwidth," in *IEEE Veh. Technol. Conf. VTC 2005-Fall*, vol. 1, Dallas, TX, Sep. 2005, pp. 372–376.

[15] J. Medbo, H. Asplund, J.-E. Berg, and N. Jaldén, "Directional channel characteristics in elevation and azimuth at an urban macrocell base station," in *Antennas and Propagation (EuCAP), Proceedings of the 6th European Conference on*, Prague, Czech Republic, Mar. 2012.

[16] A. Richter, "Estimation of radio channel parameters: Models and algorithms," Ph.D. dissertation, TU Ilmenau, Ilmenau, Germany, May 2005.

[17] M. Landmann, "Limitations of experimental channel characterisation," Ph.D. dissertation, TU Ilmenau, Ilmenau, Germany, May 2008.

[18] A. F. Molisch, *Wireless Communications*. Chichester, U.K.: IEEE Press - Wiley, 2005.

[19] B. H. Fleury, "First- and second-order characterization of direction dispersion and space selectivity in the radio channel," *IEEE Trans. Inform. Theory*, vol. 46, no. 6, pp. 2027–2044, 2000.

[20] IEEE Std 145-1993, "IEEE standard definition of terms for antennas," Antenna Standards Committee of the IEEE Antennas and Propagation Society, IEEE, Mar. 1993.

[21] R. Kattenbach, "Characterization of time-variant indoor radio channels by means of their system and correlation functions," Ph.D. dissertation, Univ. GhK Kassel, Shaker Verlag, Aachen, Germany, 1997, (in German).

[22] P.-S. Kildal and K. Rosengren, "Correlation and capacity of MIMO systems and mutual coupling, radiation efficiency, and diversity of their antennas: Simulations and measurements in a reverberation chamber," *IEEE Commun. Mag.*, vol. 42, pp. 104–112, Dec. 2004.

[23] V. Plicanic, B. K. Lau, A. Derneryd, and Z. Ying, "Actual diversity performance of a multiband diversity antenna with hand and head effects," *IEEE Trans. Antennas Propagat.*, vol. 57, no. 5, pp. 1547–1556, May 2009.